

SEVEN BROAD ABSORPTION LINE QUASARS WITH EXCESS BROAD BAND ABSORPTION NEAR 2250 Å

SHAOHUA ZHANG^{1,2}, JIAN GE², PENG JIANG³, HONGYAN ZHOU^{1,3}, JINGZHE MA², W. N. BRANDT⁴, DONALD G. YORK⁵,
PASQUIER NOTERDAEME⁶, DONALD P. SCHNEIDER^{7,8}

Draft version March 9, 2021

ABSTRACT

We report the discovery of excess broad band absorption near 2250 Å (EBBA) in the spectra of seven broad absorption line (BAL) quasars. By comparing with the statistical results from the control quasar sample, the significance for the detections are all above the $\gtrsim 4\sigma$ level, with five above $> 5\sigma$. The detections have also been verified by several other independent methods. The EBBA present broader and weaker bumps at smaller wavenumbers than the Milky Way, and similar to the Large Magellanic Cloud. The EBBA bump may be related to the 2175 Å bump seen in the Local Group and may be a counterpart of the 2175 Å bump under different conditions in the early Universe. Furthermore, five objects in this sample show low-ionization broad absorption lines (LoBALs), such as Mg II and Al III, in addition to the high-ionization broad absorption lines (HiBALs) of C IV and Si IV. The fraction of LoBALs in our sample, $\sim 70\%$, is surprisingly high compared to that of general BAL quasars, $\sim 10\%$. Although the origin of the bump is still not clear, the coexistence of both BALs and bumps and the significantly high fraction of LoBALs may indicate the bump carriers is closely related to the early evolution phase of quasars.

Subject headings: galaxies: ISM - dust, extinction - quasars: absorption lines - quasars: individual

1. INTRODUCTION

Absorption systems identified in quasar spectra are classified as “quasar-associated” or “intervening” absorbers based on the nature of absorbing materials. Compared to the origin of intervening absorbers which are produced by absorbing materials, such as intergalactic clouds or galaxies, located far from the background quasars, the origin of quasar-associated absorbers is much more complicated. While most quasar-associated absorbers are produced by materials associated with the AGN environments, a significant fraction may also be associated with AGN outflows. Therefore, quasar-associated absorbers uniquely trace a variety of regions in AGNs and their host galaxies, and their processes are closely connected to the basic physics of the central Super-Massive Black Hole (SMBH) growth and AGN evolution (Hamann & Sabra 2004 and references therein). Broad absorption lines (BALs) are the most prominent quasar-associated absorbers because of their high velocities (up to a velocity of $v \sim 0.2c$) and broad widths (at least 2000 km s^{-1} wide; see Weymann et al. (1991)).

BALs appear in the spectra of $\sim 10 - 15\%$ of optically selected quasars, and often show absorption from a wide range of species, such as Mg II, Al III and Fe II, to N V, C IV, Si IV and O VI (Hall et al. 2002; Tolea et al. 2002; Hewett & Foltz 2003; Reichard et al. 2003; Trump et al. 2006; Gibson et al. 2009; Zhang et al. 2010, 2014). BALs are clearly formed by gas outflows from the AGN central engine. The accretion of gaseous material onto the central SMBHs releases a large amount of radiative and kinetic energy to heat and expel the surrounding gas and accelerates the outflowing gas to very high velocities, producing very broad velocity profiles in the absorption lines (see Antonuccio-Delogu & Silk 2010 for a recent review). Besides the high velocities and broad line profiles, BAL quasars show remarkably weak soft X-ray emission (e.g., Green & Mathur 1996), with $\sim 10 - 30$ times less soft X-ray flux than that for unabsorbed quasars (e.g., Brandt, Laor, & Wills 2000). The apparent X-ray absorption probably implies intrinsic extinction in BALs. Previous statistical studies of optically selected BAL quasars indicate that High-ionization BAL (HiBAL) quasars as a population are not heavily reddened ($E(B - V) \sim 0.03$) while Low-ionization BAL (LoBAL) quasars show a moderate level of reddening with the average color excess of $E(B - V) \sim 0.1$ (Weymann et al. 1991; Sprayberry & Foltz 1992; Reichard et al. 2003; Gibson et al. 2009; Zhang et al. 2010). Both HiBAL and LoBAL quasars often show intrinsic dust reddening following the Small Magellanic Cloud (SMC) type as do intervening quasar absorption line systems (Reichard et al. 2003; York et al. 2006), unlike the Milky Way (MW) type dust reddening which possesses the remarkable and intriguing broad 2175 Å bump in the UV extinction curve (Stecher 1965). The bump strength increases gradually from the SMC type curve to the Large Magellanic Cloud (LMC) like curve to the MW type curve (Savage & Mathis 1979; Fitzpatrick 1989).

¹Polar Research Institute of China, 451 Jinqiao Road, Shanghai, 200136, China; zhangshaohua@pric.org.cn

²Department of Astronomy, University of Florida, Gainesville, FL, 32611, USA; jge@astro.ufl.edu

³Key Laboratory for Research in Galaxies and Cosmology, University of Science and Technology of China, Chinese Academy of Sciences, Hefei, Anhui, 230026, China

⁴Department of Astronomy and Astrophysics, 525 Davey Laboratory, Pennsylvania State University, University Park, PA, 16802, USA

⁵Department of Astronomy, University of Chicago, 5640 South Ellis Ave, Chicago, IL 60637, USA

⁶Institut d’Astrophysique de Paris, CNRS-UPMC, UMR7095, 98bis bd Arago, 75014 Paris, France

⁷Department of Astronomy and Astrophysics, The Pennsylvania State University, University Park, PA 16802

⁸Institute for Gravitation and the Cosmos, The Pennsylvania State University, University Park, PA 16802

Detections of 2175 Å features in high redshift ($z > 1$) quasar absorption line systems were first reported by Wang et al. (2004). Since then, over 40 2175 Å bumps have been found in high redshift quasar metal absorption systems, such as Mg II and Ca II (e.g., Wild et al. 2006; Srianand et al. 2008; Noterdaeme et al. 2009, 2014; Zhou et al. 2010; Jiang et al. 2010a,b; 2011; Wang et al. 2012). Despite the existence of some known 2175 Å bumps in quasar absorption line systems, they are extremely rare (York et al. 2006). They may be expected to be even more rare in regions near quasars because the carrier of the bump may not survive in the harsh UV environment close to the quasars. Indeed, only 6 quasar-associated 2175 Å absorbers are found. The measurements of metal absorption lines associated with 2175 Å absorbers suggest that the dust depletion in these absorbers is similar to that measured in cold interstellar clouds of the MW (e.g. Jenkins 2009 and references therein), which are characterized by cold, dense and primarily molecular gas (Jiang et al. 2010a,b; Zhou et al. 2010; Wang et al. 2012). This result could indicate that the carriers in these high redshift 2175 Å absorbers are likely the same as those responsible for the UV bumps in the MW and LMC.

Although the origin of the 2175 Å bump remains unclear 50 years after its discovery (Stecher 1965), carbonaceous materials have long been proposed as a candidate; a probable carrier is polycyclic aromatic hydrocarbon (PAH) molecules, the suspected source of spectral features of which are abundant in the MW (Draine 2003; Wang et al. 2005). If this is the case, then the 2175 Å bump can be detected in the quasar environment. For instance, the BAL winds can efficiently absorb the high-energy photons from the central engine of quasars to allow survival of the PAH molecules or other carriers. Extreme ultraviolet and X-ray photons can easily destroy PAH molecules (Voit 1992; Murray et al. 1995). Detections of the unidentified emission signatures in the mid-infrared spectra of six Iron Low-Ionization BAL (FeLoBAL) quasars imply that carbonaceous molecules can survive in the environments of BAL quasars (Farrah et al. 2010). However, there is no previous direct evidence of the coexistence of BALs and 2175 Å absorbers in quasar spectra.

In this paper, we report the discovery of seven possible 2175 Å absorbers in the optical spectra of BAL quasars detected in the Sloan Digital Sky Survey III (Eisenstein et al. 2009). The spectral analysis results are described in §2, discussions about the false detections are presented in §3 and 4 and conclusions and discussions are summarized in §5.

2. SPECTRA AND ANALYSIS

The spectra of these seven objects were observed in the Baryon Oscillation Spectroscopic Survey (BOSS; Dawson et al. 2013) of the third stage of the Sloan Digital Sky Survey (SDSS-III; Eisenstein et al. 2011) on a dedicated 2.5 m telescope (Gunn et al. 2006) at Apache Point Observatory (APO) in the Sacramento Mountains in Southern New Mexico. To constrain baryon acoustic oscillations (BAO), BOSS is designed to complete a spectroscopic survey of a larger volume than all of the previous spectroscopic surveys, including 1.5 million lu-

minous galaxies as faint as $i = 19.9$ with redshifts $z < 0.7$ and more than 150,000 quasar spectra ($g < 22$) over the redshift range $2.15 < z < 3.5$. The improved BOSS spectrographs (Smee et al. 2013) can observe spectra of targets two magnitudes fainter than the original SDSS spectrographs. The calibrated digital spectra cover the wavelength region of 3,600-10,500 Å at a spectral resolution in the range of $1,300 < R < 2,500$.

2.1. Searching procedures

The quasar-associated 2175 Å absorbers are rarely detected, and the generally steep extinction curve (Fynbo et al. 2013; Jiang et al. 2013) makes some objects fainter. Thus the BAL quasars with quasar-associated 2175 Å absorbers are rarer due to the additional dust reddening in the BAL clouds and their small percentage in the quasar population. Nevertheless, the improved survey sensitivity of BOSS allows detection of fainter objects with high-redshift in a larger volume than the original SDSS, offering a much larger sample of high redshift quasars to search for rare 2175 Å absorbers. Our initial exploration of 2175 Å absorbers, among Mg II absorption line systems on quasar spectra in the SDSS DR10 (Ahn et al. 2014), led to identification of excess broad band absorption near 2250 Å in seven BAL quasars.

Searching procedure of the bump exploration has three steps, and we briefly outline it here. Firstly, we construct a sample of Mg II absorbers from the SDSS DR10 quasar catalog (Pâris et al. 2013). Mg II absorbers are identified by a semi-automatic algorithm following the method of Lawther et al. (2012). Mg II absorbers have been visually inspected and some unusual absorption lines like those in Hall et al. (2002) are removed. Based on the wavelength coverage of the BOSS spectrographs and the color distribution of 2175 Å absorbers found by Jiang et al. (2011), 7950 strong Mg II absorbers with absorption redshifts of $0.7 < z_{\text{abs}} < 3.0$ and relative colors of $\Delta(g-i) > 0$, are collected as the parent sample of the exploration of 2175 Å absorbers. Secondly, we use a quasar composite spectrum reddened by a parameterized extinction curve (introduced in §2.2) to fit the observed spectra in the rest frame of absorption systems. This method is similar to the pair-method commonly used in studies of dust extinction of the MW diffuse clouds. Thirdly, we perform an independent verification approach to gauge the significance of the extinction bumps using a simulation technique developed by Jiang et al. (2010a,b; also see the last paragraph of §2.4). The bumps with a significance level of $< 3\sigma$ are considered as false candidates to be rejecting. After performing a visual examination and rejecting the false signals mimicked by greatly trimmed in the SDSS spectral data, we finally obtain 225 2175 Å absorber candidates. Among them, 25 cases are quasar-associated 2175 Å absorbers, and we find the absorption troughs of C IVBALs in the spectra of 7 objects. Figure 1 shows the spectra of these seven BAL quasars, and the fitting results of bumps in BAL quasars are presented in §2.3.

2.2. Parameterization of extinction curves

In the MW ISM studies, dust extinction curves of diffuse clouds are extracted by comparing a pair of stellar

spectra of the same spectral type, one of which is reddened and the other unreddened (Fitzpatrick & Massa 2007 and references therein). Since our technique to extract the extinction curves from quasar spectra is similar to the pair-method, we denoted our technique the “quasar spectrum pair method”. In this method, the spectrum of the target is fit using the SDSS DR7 quasar composite spectrum (Jiang et al. 2011) reddened by a parameterized extinction curve (Fitzpatrick & Massa 1990) at the optical/UV wavebands in the rest frame of the absorber of interest. The extinction curve $A(\lambda)$ is constituted by a linear background and a Drude component, representing the underlying extinction and the potential 2175 Å bump, respectively.

$$A(\lambda) = c_1 + c_2x + c_3 \frac{x^2}{(x^2 - x_0^2)^2 + x^2\gamma^2} \\ = c_1 + c_2x + c_3D(x, x_0, \gamma), \quad (1)$$

where $x = \lambda^{-1}$ is in units of inverse microns (μm^{-1}). Two parameters (c_1 and c_2) define the linear background. The Drude profile is defined by three parameters, (1) the position (in μm^{-1}) of the bump peak, x_0 ; (2) the full width at half maximum (in μm^{-1}) of the bump, γ ; and (3) the Drude profile scale factor, c_3 . The strength of the bump can be described by the area under the Drude profile, $A_{\text{bump}} = \int_0^\infty c_3D(x, x_0, \gamma) dx = \pi c_3 / (2\gamma) A_{\text{bump}} = E(B - V) \times A_{\text{bump}}^*$, where A_{bump}^* is the bump strength defined in Fitzpatrick & Massa (2007) and Gordon et al. (2003). Unlike the MW ISM studies, we do not know the intrinsic spectral slope and luminosity of the unreddened spectrum. We cannot measure the conventional extinction parameters (A_V , R_V and $E(B - V)$) from the extinction curve, derived by the comparison of the quasar spectra with the composite spectrum. Thus, $A(\lambda)$ is a relative extinction curve without normalization. Furthermore, the linear background also accounts for the variation of the intrinsic quasar spectral slopes and fluxes, and c_2 could be negative if a quasar spectrum is bluer than the composite spectrum. However, the aim of this work is to unveil the extinction bump in the quasar spectra, and the features of the extinction bump will remain the same regardless of intrinsic quasar variability. More details can be found in Jiang et al. (2011).

2.3. Fitting results of bumps in BAL quasars

In the fitting process of these seven BAL quasars, only the continuum of a quasar spectrum was fitted while the regions with strong emission lines, such as Ly α , C IV, Al III, C III and Mg II, and known strong BALs (gray curves in Figure 1) are masked without fitting. The potential excess broad band absorption is set to have the same redshift as the quasar’s emission redshift to detect the quasar-associated absorbers. We perform the least-squares minimization using the Interactive Data Language (IDL) procedure MPFIT developed by C. Markwardt.⁹ Figure 1 displays the spectra of the seven candidates with excess broad band absorption. The best fit models (green solid lines) are presented with the SDSS-III/BOSS spectrum (black curves) in panel (a). To em-

phasize the requirement of a bump on the extinction curve, we also include the reddened composite quasar spectra with only the linear component of the best fitting model (green dashed lines). The derived extinction curves are plotted in panel (a). The best fit parameters of the extinction curves of the seven candidates are listed in Table 1 and shown in panel (b) of Figure 1. Figure 2 illustrates the distribution of the absorption feature parameters and the relative extinction curves of the seven candidates. For comparison, Figure 2 also includes the bumps and the extinction curves observed in the MW (Fitzpatrick & Massa 2007; green circles and curves) and LMC (Gordon et al. 2003; red circles and curves). The peak position of the bump in the MW is nearly constant, and the bump width varies in a wide range of $\gamma = 1.0 \pm 0.25 \mu\text{m}^{-1}$. However, 7 cases in this work present broader absorption features at smaller wavenumbers ($\gamma = 1.3 \pm 0.39 \mu\text{m}^{-1}$, $x_0 = 4.45 \pm 0.05 \mu\text{m}^{-1}$ or $2250 \pm 26 \text{ \AA}$), and their bump strengths are much weaker than those of the MW bumps on average, but similar to those of the LMC bumps. The excess broad band absorbers are possibly related to the 2175 Å bump detected in our Milky Way and other galaxies. The different distributions are possibly attributed to variations in chemical composition of the grains (Draine 2003). For convenience, hereafter, we use the term excess broad band absorbers (EBBA) to refer to this new class of absorbers near 2250 Å.

2.4. Further confirmation of bumps in BAL quasars

In order to confirm the existence of the EBBA bumps, we perform continuum fitting by reddening the DR7 composite spectrum with different extinction curves, namely that from the SMC, the LMC2 Supershell (hereafter LMC2), the LMC (Gordon et al. 2003) and the MW (Fitzpatrick & Massa 2007). The 2175 Å bump is absent in the SMC extinction curve and gradually increases from the LMC2 extinction curve to the LMC and the MW extinction curves. There are two free parameters in the continuum fitting: $E(B - V)$ and a normalization scale. The results of spectral fitting are presented in Table 1. We present the best fit results using different extinction curves by blue, brown, pink and yellow curves for all the reddened quasar spectra in panel (a) of Figure 1. All objects show that the fitting reddened by a parameterized extinction curve is significantly better than those reddened by the SMC, LMC, LMC2 and MW extinction relations.

Considering that BAL quasars on average have redder continua and stronger UV and optical Fe II emission than non-BAL quasars (e.g., Boroson & Meyers 1992; Zhang et al. 2010), a few of the strongest Fe II and Fe III emission objects may be accidentally identified as 2175 Å absorbers (Pitman et al. 2000). To check the validity of the detections of the EBBA bumps, we re-fit the spectra with the composite spectrum of HiBAL quasars from Reichard et al. (2003). The fitting results are shown by red lines (solid and dashed) in panel (a) of Figure 1 and in Table 2. The HiBAL composite spectrum shows a redder continuum slope and stronger UV Fe II multiplets near the Mg II regime than the DR7 quasar composite spectrum. The derived fitting parameters are somewhat different from the results using the DR7 com-

⁹ The Markwardt IDL Library is available at <http://cow.physics.wisc.edu/~craigm/idl/idl.html>

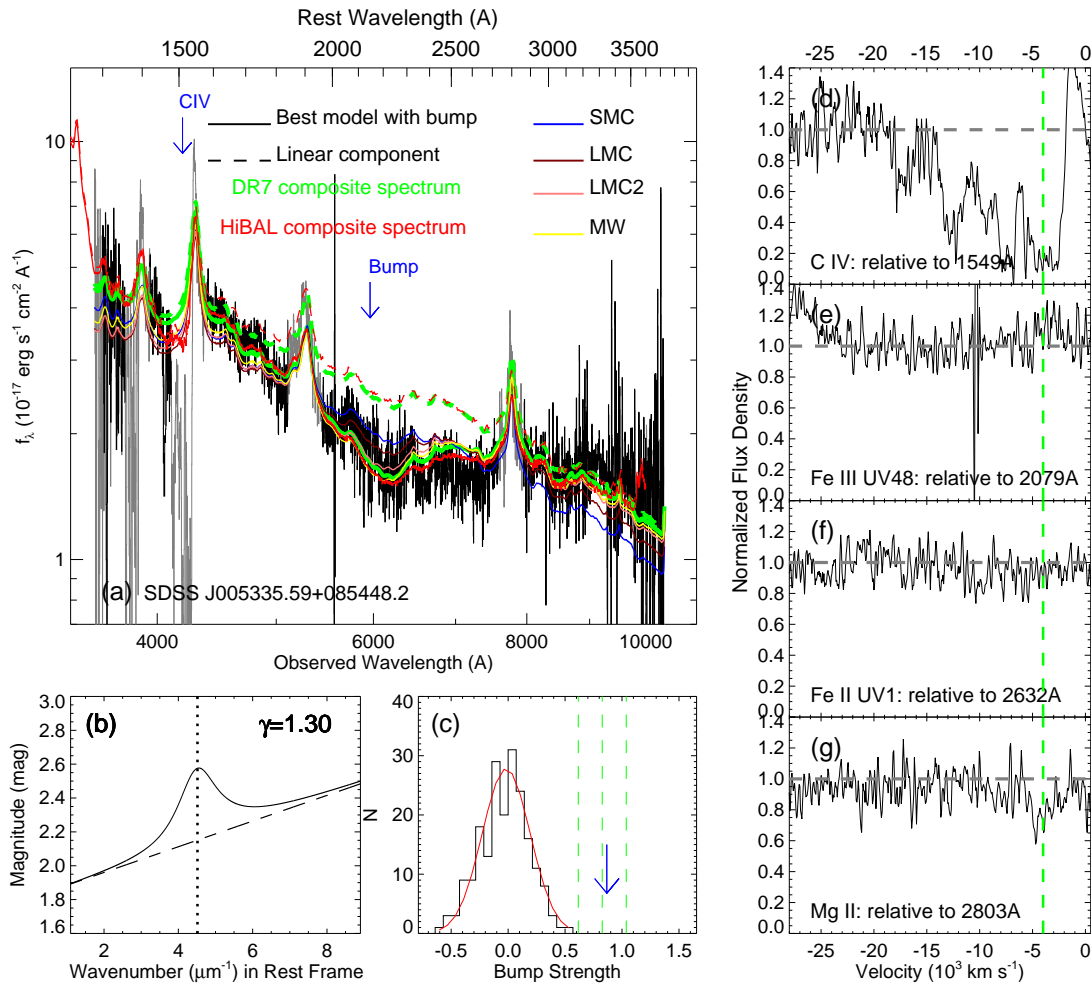


FIG. 1.— The best fit extinction model and absorption lines for J005335.59+085448.2. (a). Green solid and dashed curves are the SDSS DR7 quasar composite spectrum reddened by the best parameterized model with a linear component and a Drude component and with a linear component only, respectively. We also show the best fit results using the HiBAL quasar composite spectrum in Reichard et al. (2003) instead of the DR7 quasar composite spectrum in red. By comparison, continuum fittings with the DR7 composite spectrum reddened by the extinction curves from the SMC, the LMC2, the LMC and the MW are also plotted. The C IV BALs and the center of 2175 Å bump are marked with blue arrows. (b). The best fit result of the parameterized extinction curve for J005335.59+085448.2 (Table 1). (c). Histogram of fitted bump strength of the control sample for J005335.59+085448.2. The red line is the best fit Gaussian profile. The blue arrow indicates the strength of the bump derived from the spectrum of J005335.59+085448.2. The three vertical dashed lines are the 3, 4, and 5 σ boundaries of the Gaussian. (d-g). The normalized flux of absorption lines in velocity space.

posite spectrum. The HiBAL fitting results show slightly stronger EBBA bumps for all of the targets except SDSS J135734.05+364005.1, confirming the detections of the bump. The maximal variability of the derived bump strengths reaches $\sim 20\%$, indicating the level of uncertainties in the measured bump strengths due to the use of the different spectral template. Nevertheless, the anomalous absorption features are still clearly present.

To measure the significance level of the detections, which can also quantitatively assess the probability of false positives, we have compared the seven BAL quasar spectra with a control sample of 200 quasar spectra using the simulation technique developed by Jiang et al. (2010a,b). This approach begins with the selection of a control sample of 200 quasar spectra with an i -band signal-to-noise ratio of $SNR \geq 5$ in the range of $z_{em} - 0.05 < z < z_{em} + 0.05$, where z_{em} is the emission redshift of the studied quasar. Then we fit each spectrum by reddening the DR7 composite quasar spectrum

with a parameterized extinction curve at the absorption redshift. The parameters x_0 and γ in the parameterized extinction curve are fixed to the best values fitting the EBBA bump of interest. The “bump” strengths, which are measured from all of the best fit bumps of the spectra in the control sample, represent the random fluctuation of the quasar continuum and the variation of broad Fe II emission multiplets by assuming that no spectrum in the control sample possesses a real bump feature with the same width and peak position as the bump we detect in the candidates. The distribution of “bump” strengths is expected to be a Gaussian profile as shown by the red curve in panel (c). In principle, the bumps with a significance level of $> 3\sigma^{10}$ are considered as real candidates. All of the 2175 Å bumps reported in this paper are detected at $> 4\sigma$ and five of them are $> 5\sigma$, indicating real detections with a false positive probability of less than

¹⁰ σ is the standard deviation of the Gaussian profile.

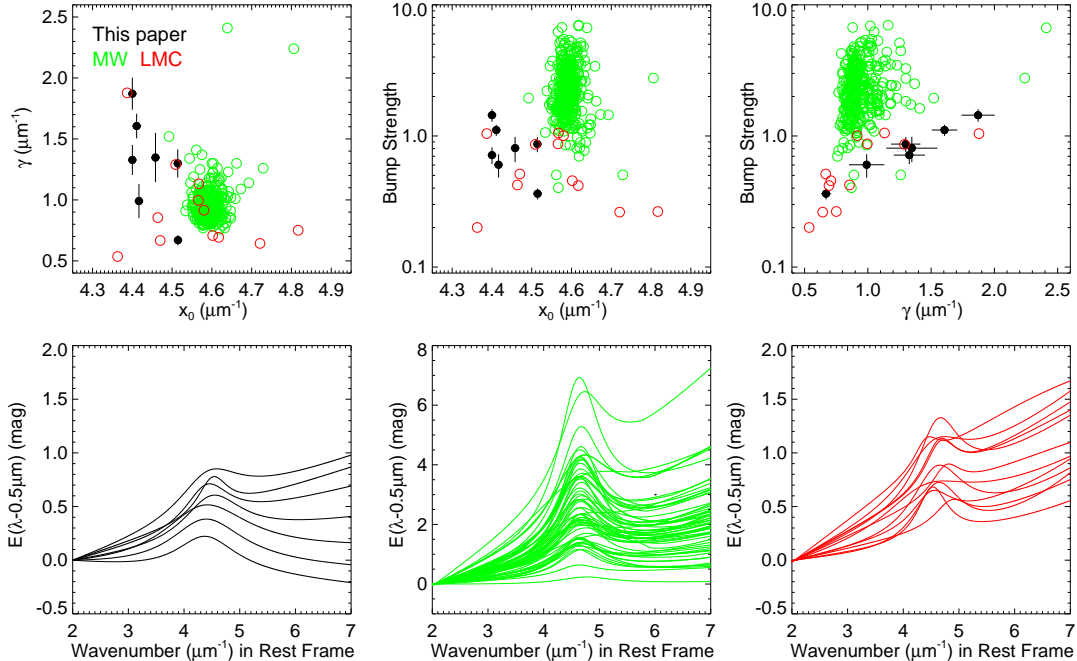


FIG. 2.— Comparison of bump parameters (top panels) and relative extinction curves (bottom panels) with 2175 Å bumps for MW (Fitzpatrick & Massa 2007) and LMC (Gordon et al. 2003) absorption curves. For visual clarity, the error bars on the MW and LMC bumps are not displayed.

0.1%.

3. POSSIBLE INFLUENCE OF BROAD IRON EMISSION

To investigate quantitatively the possible influence of broad iron emission on the bump detection, we constructed a simulated quasar sample with broad Fe II emission multiplets at different intensity levels. A total of 2,000 simulated quasar spectra without 2175 Å bumps were created using the following parameters: their redshifts are fixed to $z = 2.0$; the simulated spectra cover the rest-frame wavelength range of $\sim 1270 - 3070$ Å, matching the wavelength coverage of bump features detected in the rest frame of the BAL quasars. The simulated spectrum can be described by $f(\lambda) = f_{\text{conti}}(\lambda) + \beta f_{\text{Opt,FeII}}(\lambda) + f_{\text{err}}(\lambda)$, where $f_{\text{conti}}(\lambda)$ is the continuum plus broad emission lines, i.e., the SDSS DR7 composite quasar spectrum minus the broadened Fe II template $f_{\text{Opt,FeII}}(\lambda)$. $f_{\text{conti}}(\lambda)$ and $f_{\text{Opt,FeII}}(\lambda)$ are obtained using the spectral component separation technique introduced in Wang et al. (2009). The quantity β is a free parameter, and the equivalent width of the Fe II emission, $EW_{\text{Opt,FeII}}$,¹¹ in the simulated sample ranges from 0.0 Å to 400.0 Å. $f_{\text{err}}(\lambda)$ at each pixel is estimated from the flux density by the Gaussian error distribution, thus the signal-to-noise ratios of the simulated spectra can be matched the observed quasar sample.

This simulated quasar sample is used to search for the 2175 Å bump feature. We set the bump width at $\gamma = 0.6 + 0.1 * n$ ($n = 0, 1, \dots, 13$), $x_0 = 2175$ Å, while allow as the other parameters in Equation 1 vary freely.

¹¹ The equivalent width is measured by integrating the broadened Fe II template (Vestergaard & Wilkes et al. 2001) over 2200 Å to 3050 Å.

After the search, we obtained a false “bump” strength distribution on the two-dimensional grid surface of the bump width and strength. The influence of Fe II emission on bump detection gradually increases with EW_{FeII} and decreases with the width of the 2175 Å bumps. We derived the 3σ detection threshold for this simulated sample using the same procedure described earlier in this section and found that almost all ($> 99\%$) of the false “bumps” in the simulated spectra are under the 3σ detection threshold, except those quasars with strong iron emission (e.g., 3 times above the average iron emission strength), which are extremely rare. The most affected detections of the 2175 Å absorbers are those quasar-associated 2175 Å absorbers with narrow bumps. For comparison, our seven candidates have bumps at more than 4σ significance levels. Moreover, the first six candidates have bump widths of $\gamma \gtrsim 1.00$, and the maximal value of their Fe II emission equivalent width, EW_{FeII} of ~ 133 Å, is far less than the Fe II emission ceiling value, 270 Å, of the false detection required. Therefore, these detections are reliable. The last feature, in SDSS J232027.87+013428.2, has a narrow width of $\gamma = 0.67$ and an EW_{FeII} of 261.9 Å, slightly less than the ceiling value of 270 Å. Nevertheless, the detection level for SDSS J232027.87+013428.2 is at $\sim 4\sigma$, and the bump detection in this system is also likely to be real.

4. ARE THE EBBA BUMPS ONLY AN ILLUSION OF OTHER UNUSUAL BALS?

C IV BALs are detected in the spectra of all of the seven objects, while Si IV BALs appear in all spectra except SDSS J123852.97+420207.1. We normalized the observed spectra using the best-fit models (green solid lines in Figure 1), and measured C IV absorption lines

TABLE 1
BEST FITTED PARAMETERS AND RESULTS OF FITTING SPECTRA WITH DIFFERENT EXTINCTION CURVES USING THE SDSS DR7 QUASAR COMPOSITE SPECTRUM

Name (SDSS J)	z	$c1$	$c2$	$c3$	x_0	γ	χ_p^2	χ_{SMC}^2	χ_{LMC}^2	χ_{LMC2}^2	χ_{MW}^2
005335.59+085448.2	1.78	1.81 ± 0.01	0.08 ± 0.01	0.72 ± 0.02	4.54 ± 0.01	1.30 ± 0.12	1.06	1.60	1.43	1.26	1.20
123852.97+420207.1	2.14	2.09 ± 0.02	0.02 ± 0.01	1.72 ± 0.06	4.40 ± 0.01	1.87 ± 0.13	1.11	1.39	1.53	1.57	1.49
125101.81+052441.5	1.92	2.33 ± 0.02	-0.02 ± 0.01	1.13 ± 0.04	4.41 ± 0.01	1.61 ± 0.10	1.06	1.43	1.65	1.75	1.71
135734.05+364005.1	2.10	2.10 ± 0.02	0.13 ± 0.01	0.38 ± 0.01	4.42 ± 0.01	0.99 ± 0.14	1.19	1.40	1.24	1.22	1.30
155705.63+390805.3	2.26	1.65 ± 0.02	0.19 ± 0.01	0.69 ± 0.03	4.46 ± 0.01	1.35 ± 0.20	1.53	1.67	1.59	1.67	1.79
214653.22+004327.3	2.29	2.68 ± 0.02	-0.05 ± 0.01	0.60 ± 0.03	4.40 ± 0.01	1.33 ± 0.12	1.13	1.33	1.62	1.97	2.00
232027.87+013428.2	1.84	1.14 ± 0.01	0.17 ± 0.01	0.15 ± 0.01	4.51 ± 0.01	0.67 ± 0.04	1.11	1.55	1.15	1.13	1.29
HD 698					4.551 ± 0.006	0.96 ± 0.03					
HD 3191					4.636 ± 0.003	0.94 ± 0.02					
Cr 463-5					4.610 ± 0.008	1.08 ± 0.05					
Cr 463-18					4.606 ± 0.009	1.18 ± 0.05					
BD +57 245					4.561 ± 0.005	0.89 ± 0.03					
BD +57 252					4.577 ± 0.005	0.92 ± 0.02					
BD +70 131					4.577 ± 0.011	1.11 ± 0.05					

NOTE: χ_p^2 : Results of fitting the spectra by reddening the composite spectrum with the parameterized extinction curve and the average extinction curves of SMC, LMC, LMC2 and MW. The parameters for Galactic stars are adopted from Fitzpatrick & Massa (2007).

TABLE 2
BEST FITTED PARAMETERS WITH PARAMETERIZED EXTINCTION CURVE USING THE HiBAL QUASAR COMPOSITE SPECTRUM

Name (SDSS J)	$c1$	$c2$	$c3$	x_0	γ
005335.59+085448.2	2.09 ± 0.02	0.01 ± 0.01	1.00 ± 0.03	4.51 ± 0.01	1.43 ± 0.12
123852.97+420207.1	2.29 ± 0.02	-0.03 ± 0.01	2.32 ± 0.07	4.40 ± 0.01	2.06 ± 0.17
125101.81+052441.5	2.54 ± 0.02	-0.08 ± 0.01	1.51 ± 0.04	4.41 ± 0.01	1.77 ± 0.12
135734.05+364005.1	2.46 ± 0.02	0.06 ± 0.01	0.35 ± 0.01	4.42 ± 0.01	1.09 ± 0.14
155705.63+390805.3	1.92 ± 0.02	0.14 ± 0.01	0.77 ± 0.03	4.46 ± 0.01	1.48 ± 0.21
214653.22+004327.3	2.96 ± 0.02	-0.10 ± 0.01	0.72 ± 0.03	4.41 ± 0.01	1.46 ± 0.16
232027.87+013428.2	1.49 ± 0.01	0.10 ± 0.01	0.19 ± 0.01	4.52 ± 0.01	0.73 ± 0.14

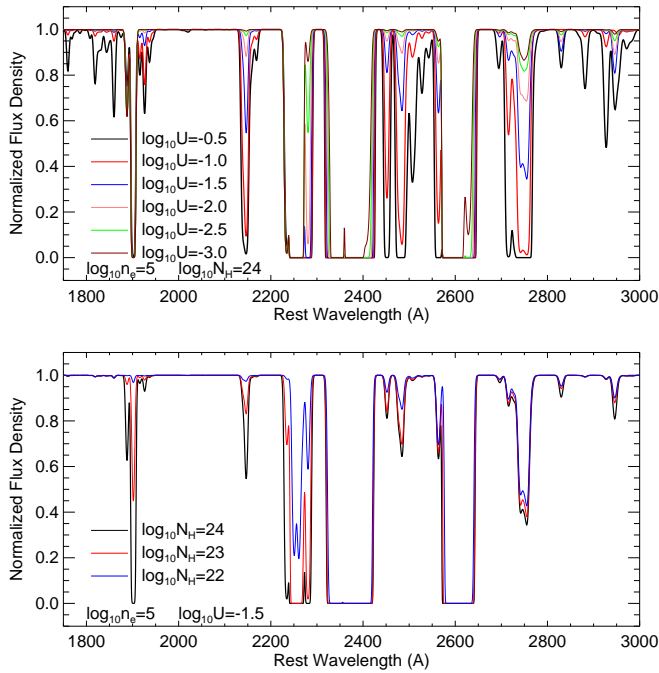


FIG. 3.— Normalized spectra of Fe II absorption lines in the 1750-3000 Å region predicted by the model using CLOUDY. In both panels, the blueshifted velocity of each Fe II absorption line is set to 0 km s⁻¹, and their widths are 1000 km s⁻¹.

TABLE 3
THE PROPERTIES OF BALs

Name (SDSS J)	Ty	V_{\min}	V_{\max}	D_{\max}	BI
005335.59+085448.2	Lo	1885	18496	0.10 ± 0.08	8701 ± 19
123852.97+420207.1	Hi	2570	5025	0.11 ± 0.07	1582 ± 4
125101.81+052441.5	Lo	1980	15589	0.00 ± 0.08	7335 ± 15
135734.05+364005.1	Lo	4743	11995	0.01 ± 0.12	5104 ± 12
155705.63+390805.3	Lo	2043	8020	0.00 ± 0.09	3944 ± 11
214653.22+004327.3	Lo	2444	11750	0.02 ± 0.09	7137 ± 8
232027.87+013428.2	Hi	8455	18482	0.26 ± 0.14	3649 ± 16

NOTE: Ty: Subtypes of BALs: Hi for HiBAL, Lo for LoBAL. V_{\min} and V_{\max} : Minimum and maximum blueshifted velocity of C IV BAL troughs from the emission line (km s⁻¹). D_{\max} : Residual flux at line bottom at the deepest part of C IV BAL troughs. BI : Balnicity Index of C IV BAL troughs (km s⁻¹), defined by Gibson et al. (2009).

in the normalized spectra (panel (d)). The balnicity index (BI) of C IV BALs are listed in Table 3. Table 3 also shows the minimal and maximal velocities of C IV BAL troughs from the emission line, the typical widths are several thousand km s⁻¹, while the maximal velocity reaches approximately twenty thousand km s⁻¹. “Balnicity” indexes are several thousands (much larger than 0) and residual fluxes in the deepest part of the troughs are close to zero, indicate the strong absorption of C IV BALs.

We classify the seven BALs in our sample as either HiBALs and LoBALs based on the modified “absorption index (AI)” introduced in Zhang et al. (2010). The AI is extracted from an observed quasar spectrum after removing absorption components from those low ionized

species such as Mg II and Al III. The unabsorbed model spectrum is obtained through multicomponent fitting of the Mg II and Al III spectral regimes. Specifically, we adopted a single power law for the continuum, two or three Gaussians for the broad Mg II and Al III lines, and the broadened UV Fe II emission multiplets (also see Lu et al. 2008) to fit the broad Mg II and Al III lines to derive their AI. The Mg II or Al III BAL troughs should fall at least 10% below the model spectrum in a contiguous velocity interval of at least 1600 km s^{-1} to be considered to be real. Based on the AI measurements, five objects are classified as LoBALs of Mg II and Al III (e.g., Mg II BALs shown in panel (g) of Figure 1). The five of BALs are marked with ‘Lo’ in Table 3, while the two remaining objects are defined as HiBALs due to lack of Mg II and Al III absorption troughs.

Since all seven objects in our sample are BAL quasars, a question is naturally raised: Are the EBBA bumps only an illusion caused by other unusual BALs, such as Fe II and/or Fe III? This confusion could occur numerous iron absorption systems cover the same broad wavelength regime as the bump, and some lines even coincidentally lie near the bump peak position. To investigate the existence of Fe II absorption, we calculated a series of models using the photoionization code CLOUDY (c10.00; Ferland et al. 1998) with different ionization parameters and hydrogen column densities, adopting the ionizing continuum from Mathews & Ferland (1987) and an electron density of $n_e = 10^5 \text{ cm}^{-3}$. In addition, the default 16-level Fe atom is used. In the top panel of Figure 3, the ionization parameter ($\log_{10}U$) is varied between -0.5 to -3.0 with a dex step of 0.5, and the highest column density is chosen to be $N_H = 10^{24} \text{ cm}^{-2}$. In the bottom panel of Figure 3, the highest column density ($\log_{10}N_H$) is set between 22 and 24 with a dex step of 1.0, and the ionization parameter is chosen to be $U = 10^{-1.5}$. The calculations suggest that the iron absorption troughs around 2400 \AA (Fe II UV 2) and 2600 \AA (Fe II UV 1) are the strongest and the most pervasive. In panel (f) of Figure 1, the normalized flux of Fe II UV1 is compared with C IV and/or Mg II BALs. The influence of Fe II BALs can be ruled out from visual examination due to the lack of detections of the commonly associated Fe II BALs in these seven spectra.

For Fe III BALs, Hall et al. (2002) reported one Fe III-dominant BAL quasar (SDSS J221511.94-004549.9) and three possible candidates (SDSS J014905.28-011404.9, J081024.75+480615.5 and J21441.43-000137.9). Fe III absorption is produced by Fe III UV48 $\lambda\lambda 2062.21, 2068.90, 2079.65$ and Fe III UV34 $\lambda\lambda 1895.46, 1914.06, 1926.30$. These four objects show unprecedented line ratios, e.g., with stronger absorption in Al III than Mg II, and FeLoBALs with weak or no Fe II but with strong Fe III, which is even stronger than Mg II. However, the troughs of Fe III UV34, Fe III UV48, Al III and Mg II have the same blueshifted velocity and similar velocity structure. Although the wavelength regime is coincidentally covered by the 2175 \AA bump, the troughs of Fe III UV34, Fe III UV48 are located well shortward of the peak position of the 2175 \AA bump. At the same time, all objects reported in this paper do not show the strong broad absorption features except the known Al III BALs around

2000 \AA (e.g., Fe III UV48 shown in panel (e) of Figure 1). Therefore, we conclude that the detected 2175 \AA bumps are unlikely to be caused by the illusion of Fe III BALs.

5. SUMMARY AND DISCUSSION

In this paper, for the first time, we report the discovery of excess broad band absorption near 2250 \AA in the spectra of seven BAL quasars. These objects were selected from the SDSS-III BOSS DR10 quasar database using the same Mg II absorption identification method reported in Jiang et al (2011). These EBBA features are detected at a high confidence level ($4-5\sigma$). They have broader widths at smaller wavenumbers, and their strengths are much weaker than those of the MW bumps on average, but similar to the LMC. The EBBA feature may be related to the 2175 \AA bump seen in the Local Group (MW, LMC, SMC) and may be a counterpart of the 2175 \AA bump under different conditions in the early Universe. If true, they are the only candidates showing both BALs and 2175 \AA -related bumps in the same spectra. Moreover, HiBALs are present in all of the seven quasar spectra while loBALs appear in five objects.

BALs are the imprints of outflows driven by supermassive black holes residing in the centers of AGNs (Weymann et al. 1991). Previous studies indicate that LoBALs may be early progenitors of normal AGNs and quasars (e.g., Farrah et al. 2007; Urrutia et al. 2009), at the very end of an extreme starburst phase. The *Spitzer* spectra of some FeLoBALs, the extreme subclass of LoBALs, have further shown significant signatures of dust and polycyclic aromatic hydrocarbon emissions (Farrah et al. 2010). Previous statistical works indicate that about 15% of quasars show BALs, and another $\sim 15\%$ of BAL quasars have detected LoBALs (Weymann et al. 1991; Hewett & Foltz 2003; Reichard et al. 2003; Trump et al. 2006; Gibson et al. 2009; Zhang et al. 2010). When we searched for 2175 \AA absorbers in the SDSS-III/BOSS DR10 quasar spectra, we identified a total of 25 quasar-associated 2175 \AA absorber candidates. Therefore, about 28% of the quasar-associated 2175 \AA absorbers show BALs, of which 71% (or five of seven) show LoBALs. Both fractions are substantially higher than those in the overall quasar sample, and the true fractions should be even higher because BAL quasars are dimmed in the observed optical wavelengths by dust reddening in the 2175 \AA absorbers and can be easily missed in a magnitude-limited sample. This situation suggests that there is a strong correlation between occurrences of LoBALs and 2175 \AA bumps. The discovery of BAL quasars with 2175 \AA -related bumps may offer a new possibility to study the connection among the central engine, the outflow of a quasar, and the dust in the host galaxy.

A probable global picture about the early evolution of quasars and their host galaxies appears from this study. The persistent processes of nucleosynthesis of the element carbon and formation of dust occur throughout the evolution of stars and galaxies, preparing the material that eventually produces the broad absorption near 2175 \AA . Dust grains with proper size and composition do not exist in all quasars. For the quasar-associated 2175 \AA or 2175 \AA -related bumps, the dusty materials are associated with

the AGN environments, probably the ISM of the host galaxy, and/or the dusty envelope layer near the quasar nucleus. In the early stage of evolution, the center of AGNs/quasars are encapsulated. When the central black holes are ignited, they release vast quantities of radiant energy, including high-energy ionizing photons (Rees et al. 1984). The radiation photoionizes and heats the surrounding gas, and drives strong outflows of gas and dust. (Davidson & Netzer 1979; Weymann et al. 1991). When the line of sight to the continuum source intersects the outflow, BALs are produced in the spectrum. Outflows can efficiently shield the high-energy photons from the central engine and extend the survival period of dust. Meanwhile, the energy feedback from outflows clears the surrounding space of the core (Silk & Rees 1998; Fabian 1999; Di Matteo et al. 2005). Accompanied by the large energy feedback, the dusty envelope layer is destroyed and cleared gradually. In this process, low-ionization ions are produced and survive in two regions, the dusty envelope layer and the core or the trailing end of outflows, because of the shielding by outflows. This appears to naturally explain the high fraction of LoBALs in the 2175 Å extinction quasars identified in this paper.

Many thanks to Dr. Xueguang Zhang and Dr. Tinggui Wang for very useful discussions and Dr. Xiheng Shi for the help with CLOUDY computations. This work is supported by the University of Florida and also Chinese Natural Science Foundation by NSFC-11203021, Na-

tional Basic Research Program of China (973 Program, 2013CB834905) and the SOC program (CHINARE2012-02-03). P.J. acknowledges supports from NSFC with grants NSFC-11233002 and NSFC-11203022. This work has made use of the data obtained by SDSS-III. Funding for SDSS-III has been provided by the Alfred P. Sloan Foundation, the Participating Institutions, the National Science Foundation, and the U.S. Department of Energy Office of Science. The SDSS-III web site is <http://www.sdss3.org/>.

SDSS-III is managed by the Astrophysical Research Consortium for the Participating Institutions of the SDSS-III Collaboration including the University of Arizona, the Brazilian Participation Group, Brookhaven National Laboratory, Carnegie Mellon University, University of Florida, the French Participation Group, the German Participation Group, Harvard University, the Instituto de Astrofísica de Canarias, the Michigan State/Notre Dame/JINA Participation Group, Johns Hopkins University, Lawrence Berkeley National Laboratory, Max Planck Institute for Astrophysics, Max Planck Institute for Extraterrestrial Physics, New Mexico State University, New York University, Ohio State University, Pennsylvania State University, University of Portsmouth, Princeton University, the Spanish Participation Group, University of Tokyo, University of Utah, Vanderbilt University, University of Virginia, University of Washington, and Yale University.

REFERENCES

- Ahn, C. P., Alexandroff, R., Allende Prieto, C., et al. 2014, *ApJS*, 211, 17
- Antonuccio-Delogu, V., & Silk, J. 2010, *Accretion and Ejection in AGN: a Global View*, 427, 343
- Brandt, W. N., Laor, A., & Wills, B. J. 2000, *ApJ*, 528, 637
- Boroson, T. A., & Meyers, K. A. 1992, *ApJ*, 397, 442
- Davidson, K., & Netzer, H. 1979, *Reviews of Modern Physics*, 51, 715
- Dawson, K. S., et al. 2013, *AJ*, 145, 10
- Di Matteo, T., et al. 2005, *Nature*, 433, 604
- Draine, B. T. 2003, *ARA&A*, 41, 241
- Eisenstein, D. J., et al. 2011, *AJ*, 142, 72
- Fabian, A. C. 1999, *MNRAS*, 308, L39
- Farrar, D., et al. 2007, *ApJ*, 662, L59
- Farrar, D., et al. 2010, *ApJ*, 717, 868
- Ferland, G. J., et al. 1998, *PASP*, 110, 761
- Fitzpatrick, E. 1989, *Interstellar Dust*, 135, 37
- Fitzpatrick, E. L., & Massa, D. 1990, *ApJS*, 72, 163
- Fitzpatrick, E. L., & Massa, D. 2007, *ApJ*, 663, 320
- Fynbo, J. P. U., Krogager, J.-K., Venemans, B., et al. 2013, *ApJS*, 204, 6
- Gibson, R. R., Jiang, L., Brandt, W. N., et al. 2009, *ApJ*, 692, 758
- Green, P. J., & Mathur, S. 1996, *ApJ*, 462, 637
- Gordon, K. D., Clayton, G. C., et al. 2003, *ApJ*, 594, 279
- Gunn, J. E., et al. 2006, *AJ*, 131, 2332
- Hall, P. B., Anderson, S. F., et al. 2002, *ApJS*, 141, 267
- Hamann, F., & Sabra, B. 2004, *AGN Physics with the Sloan Digital Sky Survey*, 311, 203
- Hewett, P. C., & Foltz, C. B. 2003, *AJ*, 125, 1784
- Jiang, P., Ge, J., Prochaska, J. X., et al. 2010a, *ApJ*, 720, 328
- Jiang, P., Ge, J., Prochaska, J. X., et al. 2010b, *ApJ*, 724, 1325
- Jiang, P., Ge, J., Zhou, H., et al. 2011, *ApJ*, 732, 110
- Jiang, P., Zhou, H., Ji, T., et al. 2013, *AJ*, 145, 157
- Lu, H., Wang, T., Yuan, W., et al. 2008, *ApJ*, 680, 858
- Mathews, W. G., & Ferland, G. J. 1987, *ApJ*, 323, 456
- Murray, N., & Chiang, J. 1995, *ApJ*, 454, L105
- Noterdaeme, P., et al. 2009, *A&A*, 503, 765
- Noterdaeme, P., Petitjean, P., Pâris, I., et al. 2014, *A&A*, 566, A24
- Pâris, I., Petitjean, P., Aubourg, É., et al. 2014, *A&A*, 563, AA54
- Pitman, K. M., et al. 2000, *PASP*, 112, 537
- Rees, M. J. 1984, *ARA&A*, 22, 471
- Reichard, T. A., Richards, G. T., et al. 2003, *AJ*, 125, 1711
- Ross, N. P., et al. 2012, *ApJS*, 199, 3
- Savage, B. D., & Mathis, J. S. 1979, *ARA&A*, 17, 73
- Silk, J., & Rees, M. J. 1998, *A&A*, 331, L1
- Smee, S. A., Gunn, J. E., Uomoto, A., et al. 2013, *AJ*, 146, 32
- Sprayberry, D., & Foltz, C. B. 1992, *ApJ*, 390, 39
- Srianand, R., et al. 2008, *MNRAS*, 391, L69
- Stecher, T. P. 1965, *ApJ*, 142, 1683
- Tolea, A., Krolik, J. H., & Tsvetanov, Z. 2002, *ApJ*, 578, L31
- Trump, J. R., et al. 2006, *ApJS*, 165, 1
- Urrutia, T., Becker, R. H., et al. 2009, *ApJ*, 698, 1095
- Vestergaard, M., & Wilkes, B. J. 2001, *ApJS*, 134, 1
- Voit, G. M. 1992, *MNRAS*, 258, 841
- Wang, J., et al. 2004, *ApJ*, 609, 589
- Wang, J., Ge, J., Hall, P. B., Prochaska, J. X., & Li, A. 2005, *IAU Colloq. 199: Probing Galaxies through Quasar Absorption Lines*, 331
- Wang, J.-G., Dong, X.-B., Wang, T.-G., et al. 2009, *ApJ*, 707, 1334
- Wang, J.-G., et al. 2012, *ApJ*, 760, 42
- Weymann, R. J., et al. 1991, *ApJ*, 373, 23
- Wild, V., Hewett, P. C., & Pettini, M. 2006, *MNRAS*, 367, 211
- York, D. G., et al. 2000, *AJ*, 120, 1579
- York, D. G., et al. 2006, *MNRAS*, 367, 945
- Zhang, S., Wang, T.-G., Wang, H., et al. 2010, *ApJ*, 714, 367
- Zhang, S., Wang, H., Wang, T., et al. 2014, *ApJ*, 786, 42
- Zhou, H., Ge, J., Lu, H., et al. 2010, *ApJ*, 708, 742

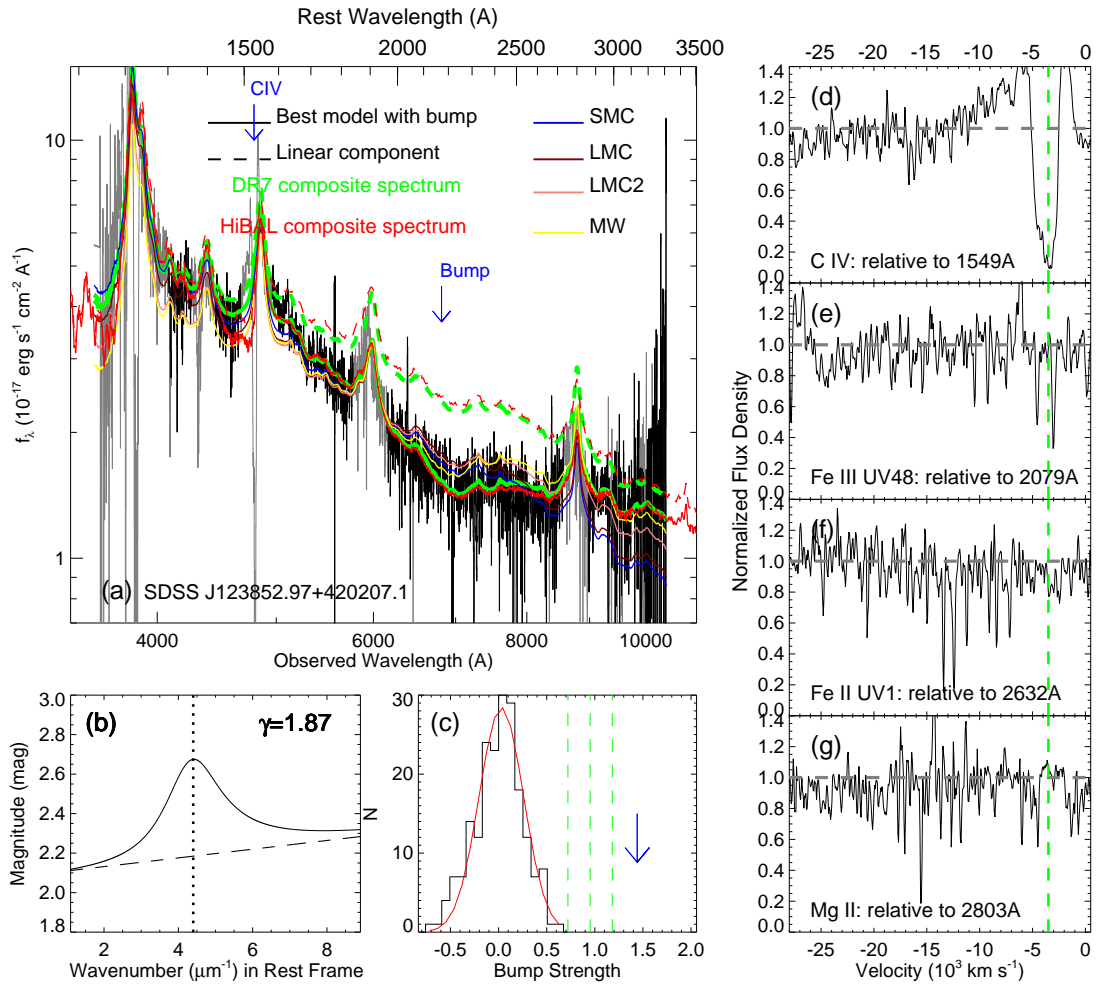


FIG. 1.— (Continued) The best fitted extinction model and absorption lines for J123852.97+420207.1.

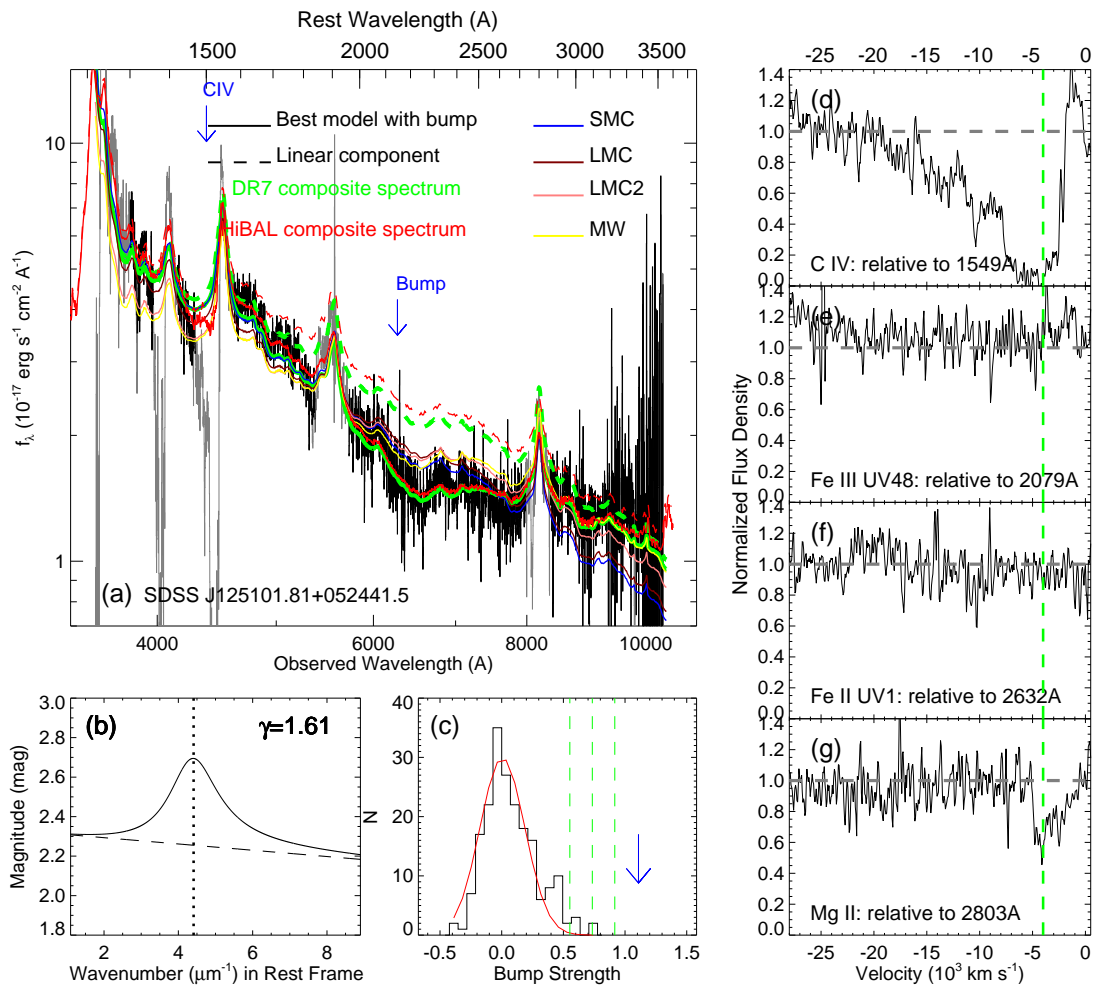


FIG. 1.— (Continued) The best fitted extinction model and absorption lines for J125101.81+052441.5.

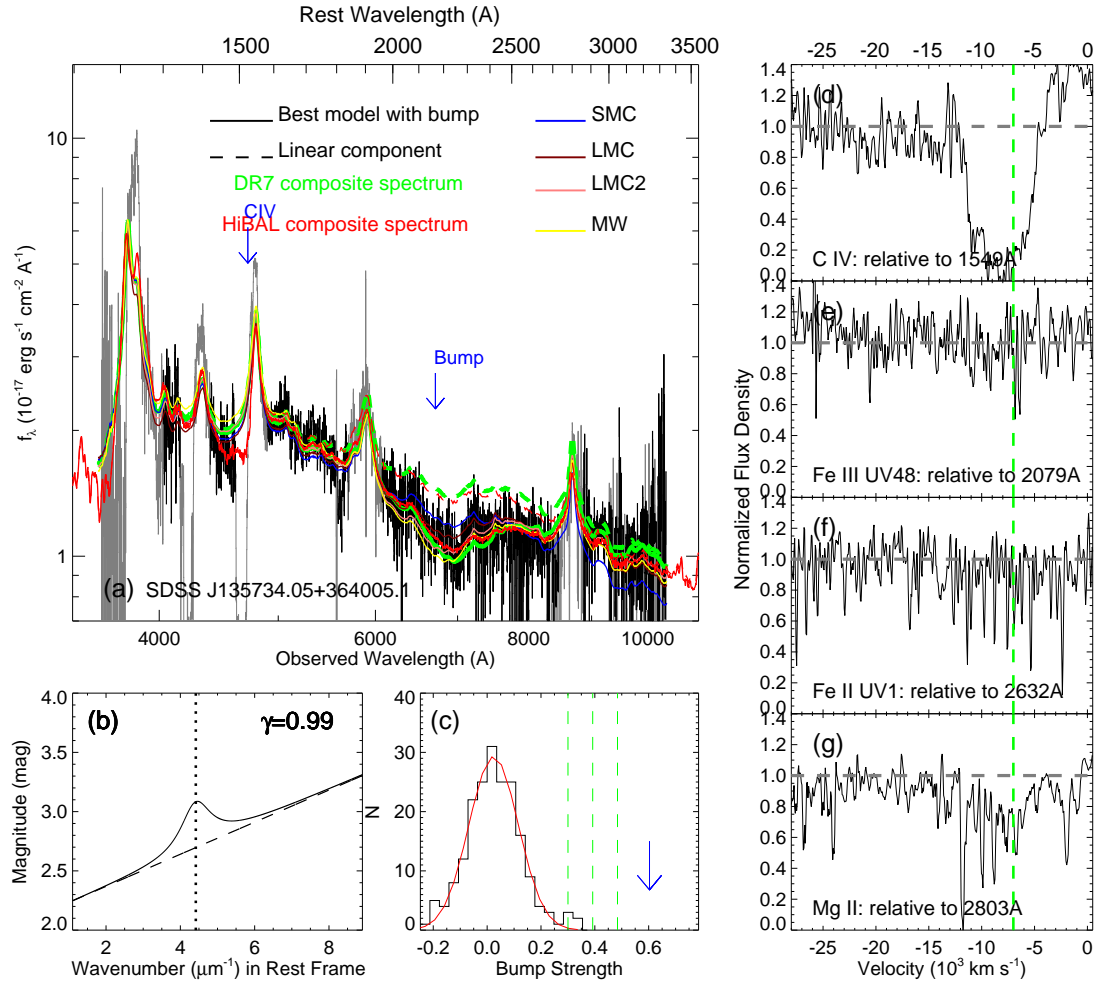


FIG. 1.— (Continued) The best fitted extinction model and absorption lines for J135734.05+364005.1.

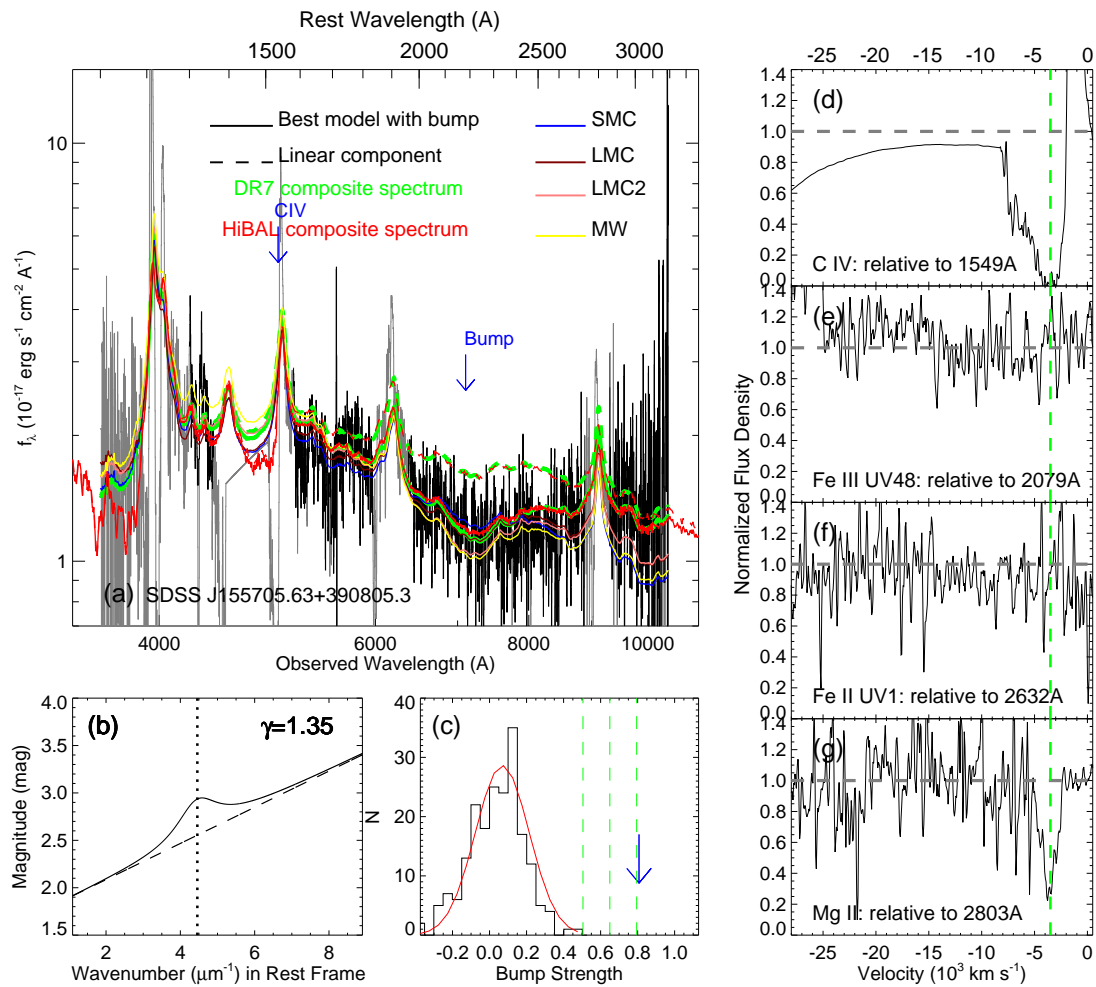


FIG. 1.— (Continued) The best fitted extinction model and absorption lines for J155705.63+390805.3.

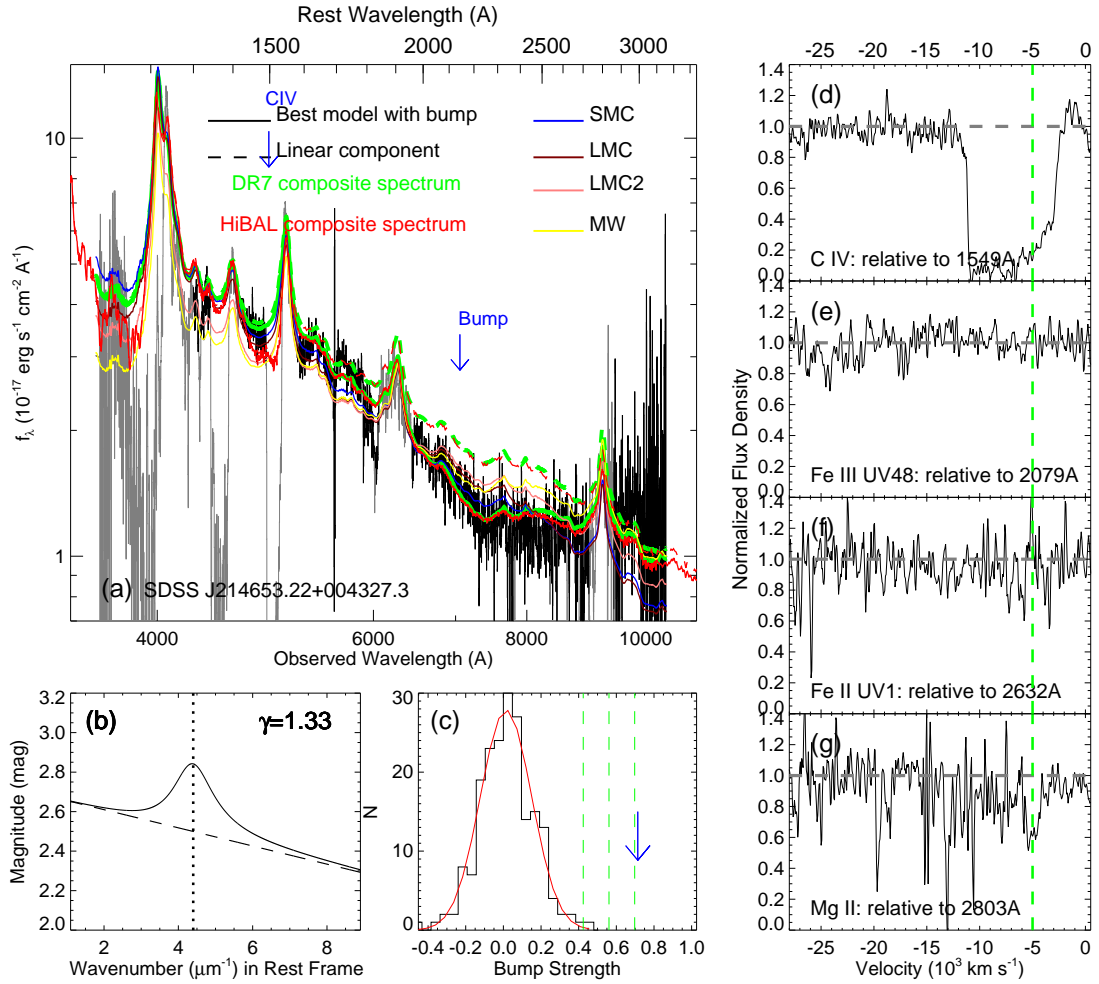


FIG. 1.— (Continued) The best fitted extinction model and absorption lines for J214653.22+004327.3.

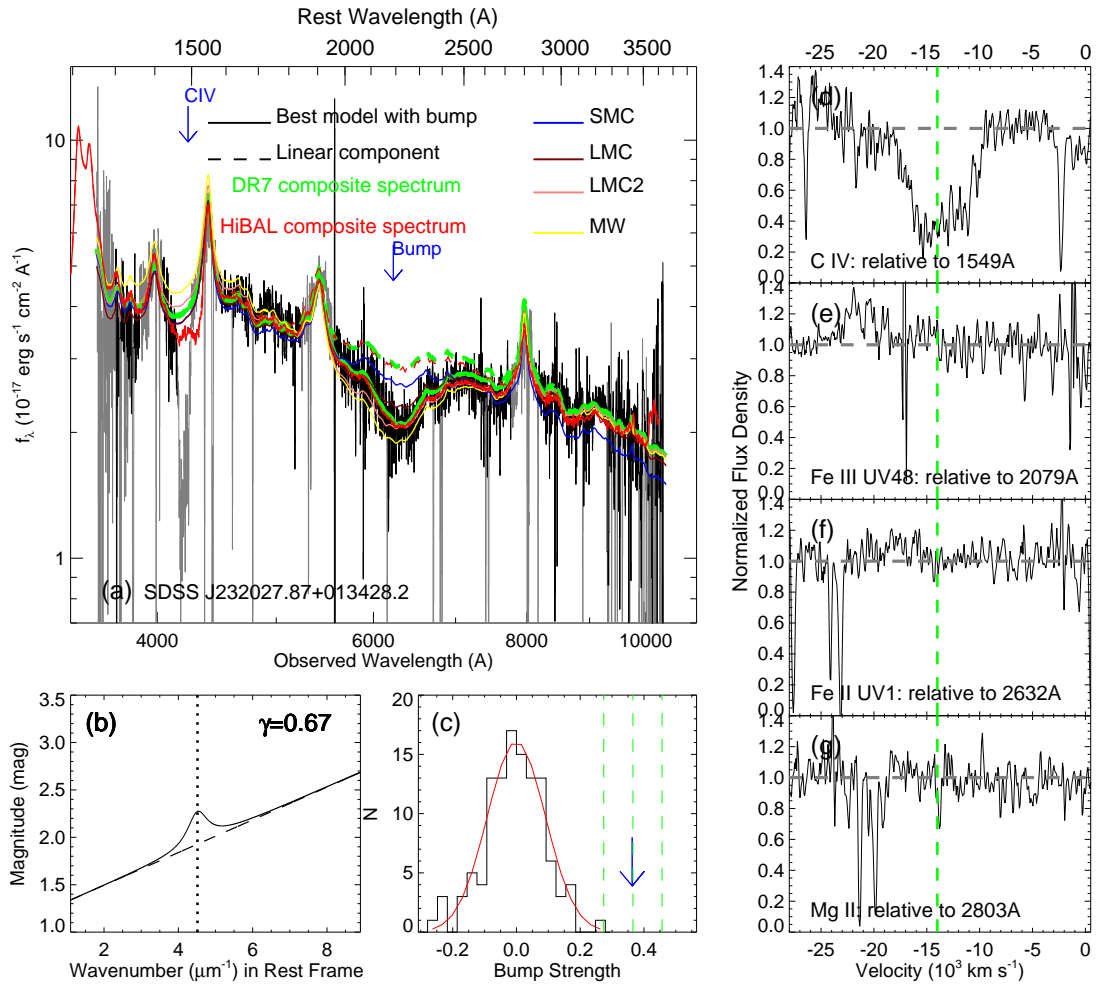


FIG. 1.— (Continued) The best fitted extinction model and absorption lines for J232027.87+013428.2.